JOURNAL OF GEOPHYSICAL RESEARCH, VOL. 95, NO. C8, PAGES 13,497–13,510, AUGUST 15, 1990

The Regional Optimization of Infrared Measurements of Sea Surface Temperature From Space

P. J. MINNETT[1]

Applied Oceanography Group, SACLANT Undersea Research Centre, San Bartolomeo, La Spezia, Italy

The accuracy with which well-calibrated satellite infrared radiometers can measure sea surface temperature is limited by the validity of the correction applied for the modification of the electromagnetic radiation before it reaches the radiometer. An accurate numerical line-by-line model of the radiative transfer through the atmosphere is used to simulate measurements of the advanced very high resolution radiometer (AVHRR/2) on the NOAA series of near-polar-orbiting satellites for conditions of the region of the Greenland, Iceland, and Norwegian Sea. A set of regionally optimized zenith-angle dependent coefficients for the "split-window" algorithm is derived and its error characteristics are discussed. While the benefit of using such coefficients is demonstrated, the errors resulting from failing to account properly for seasonal changes in this particular region are shown to be relatively small.

1. INTRODUCTION

In the decade that the advanced very high resolution radiometers (AVHRR) have been deployed on the U.S. series of near-polar-orbiting weather satellites (designated TIROS-N, NOAA 6 to NOAA 11 etc.) they have generated a continuous stream of images in the visible and infrared parts of the electromagnetic spectrum, covering the globe several times per day. One of the main uses for these data is the retrieval of quantitative measurements of the sea surface temperature (SST). The noise level of the individual infrared temperature measurements is about 0.1 K, and the AVHRR has real-time radiometric calibration, using an on-board black-body target and a view of cold space. Thus in principle, the AVHRRs should be able to provide ocean scientists and meteorologists with SST measurements of good accuracy and coverage superior than that possible by any other means. The problem, however, is that in its passage through the intervening atmosphere the radiation leaving the sea surface is significantly modified in a way that is highly variable in space and time. The accuracy of the spaceborne measurement of SST using a self-calibrating instrument is therefore limited by the accuracy with which the effect of the atmosphere can be corrected.

The commonly used method of correcting for the atmospheric effects is to combine measurements made at different wavelength intervals (channels) at which the atmospheric influence is different. The correct algorithm for combining these multichannel measurements is dependent on the range of atmospheric conditions. Thus for studies in which only a restricted set of atmospheric conditions is met, such as in a limited region over a limited period, a different algorithm may be more appropriate than one designed to cope with the full range of atmospheric variability, or a different regional or seasonal subset of atmospheric conditions. For example, *Llewellyn-Jones et al.* [1984] made the distinction between algorithms suitable for use in temperate (North Atlantic) or tropical conditions. Subsequently, *Minnett* [1986] showed that the application of different regional algorithms produced varying levels of inaccuracy when applied to a test set of simulated AVHRR measurements in summer conditions of the North Atlantic marine atmosphere.

It is the purpose of this study to methodically investigate the relative benefits, if any, that are to be gained in going from a globally applicable algorithm to one that has been optimized for certain regional and seasonal conditions. The method chosen is to use simulated satellite measurements produced by an accurate line-by-line model of the radiative transfer through the atmosphere, and the area chosen for the regional optimization is the Greenland-Iceland-Norwegian (GIN) Sea [*Minnett*, 1988]. While the numerical results are directly applicable to this area, or to other areas with similar atmospheric conditions, the general conclusions should be valid for regional studies elsewhere. This study is directed at the so-called "split-window" SST algorithm of the AVHRR/2, flown on the NOAA 7, NOAA 9 and NOAA 11 satellites, that have two distinct channels (Channels 4 and 5) in the 10- to 13-μm atmospheric window.

Following this introduction, a general discussion of the merits of different methods of determining the coefficients of an SST retrieval algorithm is given; this is followed by a summary of radiative transfer in the atmosphere, and then the numerical model is briefly described. The split-window SST retrieval expression is discussed in section 5; section 6 presents the environmental variables used to characterize the relevant conditions in the GIN Sea area, and section 7 gives a very brief description of the AVHRR. The results of the simulation study are presented in section 8 and this is followed by the summary and conclusions (section 9).

[1]Now at Brookhaven National Laboratory, Upton, New York.

Paper number 90JC01039.
0148-0227/90/90JC-01039$05.00

2. SEA SURFACE TEMPERATURE RETRIEVALS

In the "thermal infrared" part of the electromagnetic spectrum, where these satellite measurements are made, the atmospheric effect is wavelength dependent (Figure 1). In practice, the algorithm for correcting for atmospheric effects in the measurement of SST takes the form of a simple linear combination of the temperatures measured in the different channels, T_i:

$$T_s = a_0 + \sum_{i=1}^{n} a_i T_i \qquad (1)$$

where T_s is the SST measurement, a_i are dimensionless coefficients, n is the number of channels, and a_0 is a constant temperature [e.g., *Prabhakara et al.*, 1974; *McMillin*, 1975; *McMillin and Crosby*, 1984]. The minimization of errors in the SST measurement is dependent on the correct choice of the coefficients a_0, a_i.

There are two approaches to determine the coefficients, and these can be conveniently referred to as the empirical and the simulation methods. The empirical approach requires the collection of high-quality measurements from in-situ thermometers, such as on drifting meteorological buoys, that are coincident with satellite measurements, and then a regression analysis of the in-situ temperatures and the satellite data produces the coefficients. The alternative approach uses a computer model of atmospheric radiative transfer together with a large set of atmospheric profiles to simulate the satellite measurements in a range of conditions. The simulated measurements are then used with a set of assigned SST values to derive the coefficients, again by regression analysis. In both methods, the regression analysis also provides an estimation of the accuracy with which the SST value can be derived.

The advantage of the empirical method is that it uses real satellite data and real in-situ data in real conditions. It does, however, have some disadvantages:

1. The satellite measurement is of the radiation temperature, which, after correction for the atmospheric effect, is attributable to the surface "skin" of the ocean, while the in-situ measurement is generally taken at a depth of a few centimeters to a few meters (the so-called "bulk" temperature). Because of the heat exchange between ocean and atmosphere, the surface skin temperature is generally several tenths of a kelvin colder than the bulk temperature. This "skin effect" is highly variable [*Robinson et al.*, 1984]. There are some in-situ measurements from research ships taken with radiation thermometers [e.g., *Schluessel et al.*, 1987] but they are quite scarce.
2. Spatial and temporal variability in the SST field introduces uncertainty into the comparison: the satellite measurement is a near-instantaneous spatial average, whereas the in-situ measurement is either a point sample, a temporal average at a given location, or a temporal and spatial average along a ship's track.
3. The number of usable coincident sets of measurements is relatively small because many are invalidated by the effects of clouds in the satellite data. For example, in an operational SST retrieval procedure, *McClain et al.* [1985] report that typically less than 2% of the AVHRR data remain after the successive application of various cloud detection tests. Generally, the condition of coincidence must be relaxed to include in-situ

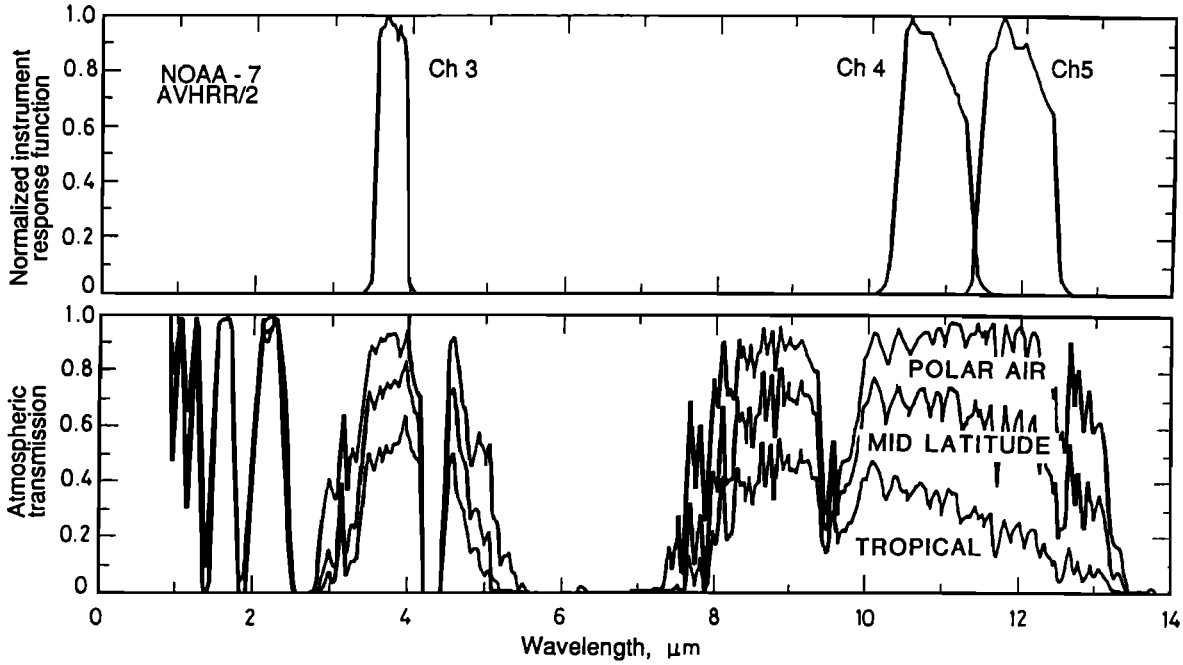

Fig. 1. Theoretical spectra of atmospheric transmission, at nadir, in the infrared region at 1- to 14-μm wavelength. The three spectra correspond to different amounts of precipitable water (polar, 7 mm; temperate, 29 mm; tropical, 54 mm). The reponse functions of channel 3 ($\sim$ 3.7 μm), channel 4 ($\sim$ 11 μm) and channel 5 ($\sim$ 12 μm) of the AVHRR/2 on the NOAA 7 satellite are shown. The different dependence of atmospheric transmission on water vapor amounts in each channel permits an estimate of the atmospheric effect in sea surface temperature measurement by multichannel methods.

temperatures taken within several hours of the satellite overpass, thus introducing the possibility of errors caused by temporal or advective temperature changes.

4. The presence of undetected clouds in the satellite data is a source of error.

5. Calibration errors in both the satellite and in-situ data are carried over into the SST retrieval expression.

The simulation approach is shown schematically in Figure 2. It avoids all of the problems of the empirical approach, but is prone to disadvantages associated with the model and its input:

1. Errors can arise through inadequate knowledge of the spectral properties of the atmospheric constituents and their dependences on temperature and pressure, which is especially relevant to the water vapor "spectral continuum," and through assumptions necessary in the formulation of the numerical model, such as the effects of aerosols.

2. Measurement errors in the atmospheric profiles will introduce errors in the simulated satellite data. Random measurement errors in individual profiles are not important, provided the profile remains physically realistic, as the data are used to represent realistic distributions rather than the true state of the atmosphere at the time and location of each profile.

3. Since the simulations are of skin temperature measurement, the predictions of the modelling, i.e., the coefficients of the retrieval expression and its accuracy, are difficult to verify properly. Discrepancies in predictions and validation data could be caused by several effects which may not be readily identifiable.

The main advantage of the simulation approach is that it permits controlled numerical experiments to investigate the behavior of the predicted algorithm in response to variations in the input information. In particular, one can study its response to different atmospheric conditions (such as those caused by regional and seasonal variations) or its dependence on particular variables, such as the satellite zenith angle.

The simulation approach is adopted here, largely because of this advantage, but also because it avoids the need for collecting and controlling the quality of large quantities of in-situ data and processing the large number of corresponding satellite images. The empirical approach is also rendered unfavorable because the area of interest, the Greenland–Iceland–Norwegian Sea (GIN Sea), is one with a relative paucity of ships and buoys.

3. RADIATIVE TRANSFER IN THE ATMOSPHERE

The energy received by a satellite radiometer directed toward the sea surface has components originating from the sea, the atmosphere, and the Sun. In the atmosphere, the processes of absorption, emission and scattering are caused by both molecules and suspended particles, such as dust, water droplets, ice crystals and sea salt crystals. By confining ourselves to a relatively narrow wavelength interval in the infrared part of the electromagnetic spectrum, the only significant components of the radiation received by the satellite radiometer are (1) the radiation emitted at the sea surface, but modified by its passage through the atmosphere; (2) the radiation emitted by the atmosphere (including aerosols) into the radiometer field of view; and (3) the radiation emitted by the atmosphere (and aerosols) and reflected at the sea surface into the radiometer field of view.

Thus

$$L_H(\nu) = L_0(\nu)\exp[-\tau(0,H)] + \int_0^H L_A(z,\nu,T_A)\kappa(z,\nu)\exp[-\tau(z,H)]\,dz \tag{2}$$

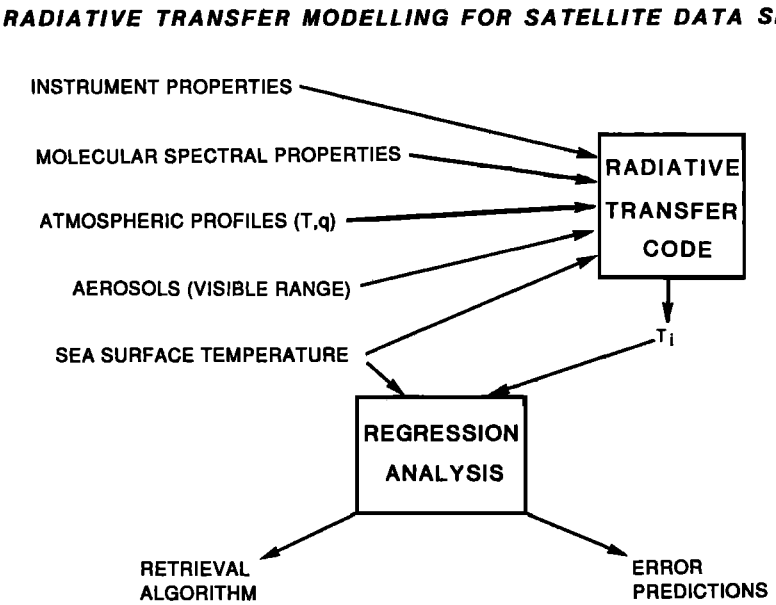

Fig. 2. Block diagram of the procedure for the numerical simulations of satellite radiometric measurements.

where $L_H(\nu)$ is the spectral radiance measured at the satellite at height H above the sea surface, $L_0(\nu)$ is the upwelling spectral radiance at the bottom of the atmosphere, L_A is the spectral radiance emitted by the atmosphere at apparent temperature T_A, and

$$\tau(z_1, z_2) = \int_{z_1}^{z_2} \kappa(z')dz' \tag{3}$$

is the optical thickness of the layer $z_2 - z_1$. When $z_1 = 0$ and $z_2 = H$, τ is the optical depth of the atmosphere. The zenith angle dependence is implicit in all terms.

The term $L_0(\nu)$ is the sum of the radiation emitted by the sea surface at temperature T_s and the reflected downwelling atmospheric radiation,

$$L_0(\nu) = \epsilon(\nu)B(T_s, \nu) + \big(1 - \epsilon(\nu)\big) \times \int_H^0 L_A(z, \nu, T_A)\kappa(z, \nu)\exp\big[-\tau(z, 0)\big]dz \tag{4}$$

where $\epsilon(\nu)$ is the emissivity of the sea surface, and B is Planck's function

$$B(T, \nu)d\nu = \frac{2h\nu^3 d\nu}{c^2\big(e^{h\nu/kT} - 1\big)} \tag{5}$$

where h is Planck's constant, k is Boltzmann's constant and c is the speed of light in vacuum.

In order to simulate real satellite measurements, it is necessary to integrate the spectral radiance at satellite heights, $L_H(\nu)$, across the width of the channel, using $\phi_i(\nu)$, the spectral response for channel i, to give the channel radiance L_i,

$$L_i = \int_0^\infty L_H(\nu)\phi_i(\nu)d\nu \Big/ \int_0^\infty \phi_i(\nu)d\nu \tag{6}$$

Throughout the atmosphere, emission and absorption are dependent on the local temperature, on the density of aerosols, on the density of molecular types composing the gaseous atmosphere, and on the spectral properties of those molecules, which in turn are temperature and pressure dependent. The atmospheric molecules of interest are water vapor (H_2O), carbon dioxide (CO_2), ozone (O_3), nitrous oxide (N_2O) and methane (CH_4).

With the exception of water vapour, the atmospheric gases listed above can be considered "well mixed" throughout the atmosphere and not to exhibit significant seasonal or regional changes. There is a well-documented seasonal variation in the concentration of CO_2 [e.g., *Hanson et al.*, 1981], but with a relatively small amplitude of $< 5\%$ of the mean value of 330×10^{-6}, and this variation can be safely neglected because it is water vapor that dominates the atmospheric effect at the wave number interval of interest.

The concentration of atmospheric water vapor exhibits extreme variations which must be correctly accounted for in numerical simulations. Water vapor adds a further complication, as in addition to the line absorption and emission of infrared radiation by molecular rotation and vibration, it displays quasi-continuous absorption and emission which is dependent on the water vapor pressure. This has been termed the "water vapor continuum" and is presumed to be caused by the presence of water vapor dimers, $(H_2O)_2$, and possibly larger water vapor polymers. The continuum effects form an important part of the total atmospheric contribution to the satellite radiometer signal, especially for moist atmospheres, and although there are experimental determinations of the properties of the water vapor continuum, uncertainties in these are likely to contribute a significant component to the inaccuracies in numerical simulations [*Barton et al.*, 1989].

Even thin clouds in the radiometer field of view prevent the infrared radiation from the sea surface reaching the height of the spacecraft. Thus as for measurements made using visible wavelengths, the clouds obscure the sea surface when observed from satellites. Consequently, for the purposes of these simulations it is presumed that effective data analysis techniques exist to identify all pixels in the infrared image data that contain any cloud [e.g., *Bernstein*, 1982; *Coakley and Bretherton*, 1982; *Crosby and Glasser*, 1978; *Llewellyn-Jones et al.*, 1984; *McClain et al.*, 1985; *Minnett et al.*, 1984; *Phulpin et al.*, 1983; *Saunders*, 1986; *Saunders and Kriebel*, 1988]. These contaminated pixels must be excluded from the procedure to retrieve accurately sea surface temperature.

For the simulations discussed here, the atmospheric temperature structure is described by sets of radiosonde profiles [*Minnett et al.*, 1986, 1987], but profiles from other sources, such as from satellite-borne atmospheric sounders, or standard atmospheres, or even synthetic profiles could be used.

The density of aerosols exhibits much spatial and temporal variability and must be well described for the purposes of the simulations. In the cases discussed here only tropospheric aerosols in the lowest 1 km of the atmosphere are considered, and these are parameterized in terms of the sea level horizontal meteorological range (see section 6.3 below). The similarity in size between the wavelength of the infrared radiation and some aerosol particles means that they can be effective scatterers. Assuming the aerosol particles to be spherical, Mie theory can be used to calculate extinction coefficients for a variety of aerosol types and concentrations [*Kneizys et al.*, 1980]. In conditions where the density of aerosols is sufficiently high for multiple scattering to be important, it is assumed that the cloud detection algorithms of a sea surface temperature retrieval procedure would identify such cases as not being "clear-atmosphere" measurements. Consequently, multiple scattering by aerosols is neglected here.

A fuller discussion of atmospheric radiative transfer is given elsewhere [e.g., *Kondratyev*, 1969; *Tiwari*, 1978].

4. THE RADIATIVE TRANSFER MODEL

The computer model used here is derived from a general radiative transfer code developed at the Rutherford Appleton Laboratory (RAL) of the UK Science and Engineering Research Council and made specific

for the spectral intervals of the "atmospheric windows" at wavelengths of 10 to 13 μm, which are used by AVHRR/2 (Figure 1). The computer model itself has been previously validated [*Llewellyn-Jones et al.*, 1984] in that sea surface temperature retrieval coefficients for North Atlantic conditions, derived entirely from the model simulations, produced SST values with reasonable error characteristics (i.e., mean error $\sim$ 0.1 K, rms $\sim$ 0.6 K) when compared with in-situ data from research ships. These errors are comparable to, if not better than, those of other sets of retrieval coefficients found in the literature. Furthermore, the zenith angle dependence of the coefficients from the model agree with physical expectations [*McMillin and Crosby*, 1985].

The model simulates the atmospheric radiative transfer with a wave number increment of 0.04 cm^{-1} and treats each spectral line in the atmospheric window individually; i.e., it is a line-by-line model, as opposed to band models in which only the mean properties of all the spectral lines of a larger wave number interval (say 20 or 40 cm^{-1}) are considered.

The spectral data describing the radiative attenuation of the atmospheric gases have been precalculated at each wavenumber increment at five standard levels in the atmosphere. These are at pressures of 1000, 800, 600, 400, and 200 mbar, with corresponding temperatures of 290, 280, 270, 250 and 220 K. The properties of each spectral line have been taken from the U.S. Air Force Geophysics Laboratory compilation [*Rothman*, 1981], using the *Gross* [1955] line shape for collision broadening. All spectral lines within 20 cm^{-1} wave numbers of each wave number increment are considered. A total of 908 spectral lines are used for the wave number interval for AVHRR/2 channel 4 and 925 for channel 5. The channel 4 interval begins at 853.76 cm^{-1} and has 3656 increments, and channel 5 begins at 800.00 cm^{-1} with 2222 increments. At each wave number increment and at each of the five standard levels, the attenuation coefficient and its temperature dependence (parameterized in terms of a quadratic function of temperature difference) have been calculated and stored as two sets of values, one for water vapor and the other for the well-mixed gases. The quadratic parameterizations are used to calculate the attenuations at the measured temperature, but at the nearest two of the standard pressures. Then linear interpolation, or extrapolation, in pressure provides the required attenuation at the measured temperature and pressure.

The water vapor dimer attenuation, the so-called continuum or anomalous attenuation, is derived from a parameterization of the form

$$\tau_2 = \alpha \rho_w^2 \exp[\gamma/(T - T_0)] \tag{7}$$

where α is an empirically determined quadratic function of wave number [*Bohlander*, 1979], ρ_w is the water vapor density, γ is a constant, T is the measured temperature, and T_0 is a reference temperature (296 K).

The atmosphere is considered to consist of 128 plane-parallel layers of uniform pressure intervals of about 8 mbar. The precise pressure resolution is dependent on the value of the surface pressure. For the simulation of measurements through atmospheric paths at zenith angle θ, the thickness of each layer is multiplied by $\sec\theta$. For zenith angles less than $\sim$60°, refraction by the stratified atmosphere can be neglected and θ can be considered a constant, as is the case in the simulations discussed here. For larger zenith angles, refraction becomes progressively more important and must be taken into account [e.g., *Kondratyev*, 1969].

Measurements of atmospheric temperature and humidity profiles are much more numerous than those of aerosol properties. Consequently it is necessary to adopt a model of the aerosol distribution and properties. For the simulations discussed here it is assumed that the aerosols are confined to the lowest kilometer of the atmosphere (which is similar to some assumptions used elsewhere [e.g., *Kneizys et al.*, 1980]) and that the aerosol extinction (i.e., scattering plus absorption) coefficient β is scaled by the sea level horizontal meteorological range V as given by the Koschmieder formula

$$V = \frac{1}{\beta} \ln \eta^{-1} = 16.99/\beta \tag{8}$$

where the coefficient β is for a reference wavelength of 0.55 μm and has units of decibels per kilometer and η is a constant, set to 0.02.

Throughout the lower kilometer the extinction coefficient is itself scaled by the measured profile of relative humidity u according to the results of *Hänel* [1976],

$$\beta \propto \left(\frac{1-u}{1-u_0}\right)^m \tag{9}$$

where u_0 is the relative humidity at sea level, and m is a constant, set to 0.4. To extend these expressions to the wavelength intervals of interest here (10 to 13 μm) the normalized extinction coefficient $\hat{\beta}_\lambda$ at 11 μm for the marine aerosol type of the LOWTRAN-5 code were used [*Kneizys et al*, 1980; Appendix A, pp. 180–183] to give

$$\beta_\lambda = \frac{16.99}{V} \left(\frac{1-u}{1-u_0}\right)^{0.4} \hat{\beta}_\lambda \tag{10}$$

A similar expression is used to obtain the aerosol emission coefficients.

At the 10- to 13-μm wavelength interval, aerosol effects are much less important than at shorter wavelengths, so the simulations are relatively insensitive to inadequacies in the aerosols model. It has been shown elsewhere [*Minnett*, 1986] that for the atmospheric conditions typical of the mid-latitude summer, changing the meteorological range from 100 km to 23 km changes the predicted measured temperatures, T_4 and T_5 (where the subscripts refer to the AVHRR/2 channel numbers; see Table 3 below), by less than about 0.4 K. This is to be compared with mean temperature deficits (for 100 km range) of 1.8 K (for $T_s - T_4$) and 2.7 K (for $T_s - T_5$).

The atmospheric attenuation at each wave number and pressure increment is then calculated as the sum of those from the water vapor monomer, the water vapor continuum, mixed gases, and aerosols. By summing the effects at each pressure increment, the model can now produce three spectra for each atmospheric profile:

the atmospheric attenuation, the upwelling atmospheric radiance at the satellite height, and the downwelling atmospheric radiance at the bottom of the atmosphere. These are independent of the sea surface temperature itself and of the properties of the particular satellite radiometer.

The next step in the simulation is to calculate the emission from the sea surface in the required wave number interval at a given sea surface temperature and combine this with the model outputs to give the upwelling radiance spectrum at the satellite height. Since the air-sea temperature difference is a variable quantity, it is legitimate to use a set of SST values with each atmospheric profile. The choice of SST values should, of course, be guided by geophysical constraints (see section 6.2 below).

Finally, the simulated satellite radiance measurement is derived by summing the product of the calculated upwelling radiance at each wave number increment and the corresponding element of the normalized channel response function. The result can be expressed as the measured channel temperature (T_4 or T_5 for the case of the AVHRR/2 longwave channels) by inverting the Planck function, taking into account the channel response function.

For the purposes of retrieval algorithm development, the simulations of the satellite measurements are done for a large set of atmospheric profiles, each with a range of air-sea temperature differences, to provide a representative set of T_4, T_5, and T_s. It has been shown that to adequately describe the range of atmospheric and oceanic conditions in a regional and seasonal study, about 500 sets of simulated measurements are required [*Minnett*, 1986]. This can be satisfied by using 100 independent profiles to correctly sample the atmospheric variability, each with five different air-sea temperature differences.

5. THE "SPLIT-WINDOW" RETRIEVAL

The transfer functions for the infrared channels of the NOAA 7 satellite AVHRR/2 are shown in Figure 1, and there are slight differences between the channel transfer functions from satellite to satellite. The two channels of interest are 4 and 5, which share the atmospheric window at 10- to 13-μm, and thus they are sometimes called the "split-window" channels. This is at the peak of the Planck function for marine surface temperatures. The spectral proximity of the channels supports the assumptions needed to linearize the radiative transfer problem and derive the multichannel retrieval expression, which can be written

$$T_s = a_0(\theta) + a_4(\theta)T_4(\theta) + a_5(\theta)T_5(\theta) \qquad (11)$$

where θ is the local zenith angle to the satellite sensor measured at the sea surface. The zenith angle dependence is required not only because of the changes in atmospheric path length across the instrument swath, but also because of the dependence of the sea surface emissivity ϵ on emission angle. The surface emissivity, weighted by the normalized channel transfer functions, is smaller for channel 5 than for channel 4 at all emission angles.

The atmosphere is generally cooler than the ocean surface below, and as a result the temperatures measured in space are usually lower than the sea surface temperature. Further, since the atmosphere is less transparent for channel 5 than for channel 4, the atmospheric contribution to the channel 5 signal is greater, and thus T_5 is lower than T_4. Meteorological situations do arise where the reverse is true, and these are caused by warm, moist layers in the atmosphere being advected over a cooler ocean surface. However, cases with $T_5 > T_4$ are very rare, as the atmospheric temperature inversion has also to overcome the effect of the inevitably colder atmosphere above as well as the effects of the lower surface emissivity at channel 5.

The coefficients for the split window retrieval expression are determined by simple linear regression analysis of the simulated measurements. This must take into account the possibility of inherent noise in the radiometer channels which can be assumed to have a Gaussian distribution about zero mean. The derived retrieval coefficients a_i are thus dependent on the noise levels of the radiometer channels.

6. ENVIRONMENTAL VARIABLES

The various environmental parameters that characterize the GIN Sea area are discussed in this section. Since it is these variables that represent the regional conditions in the simulations, much attention must be given to ensuring that they represent fairly the true physical situation; otherwise, the whole simulation exercise for a regional study could be invalidated.

6.1. *Atmospheric Profiles*

The profiles of atmospheric temperature and moisture used here have been measured by radiosonde ascents, and are a subset of North Atlantic area profiles selected from the extensive archive at the U.K. Meteorological Office [*Minnett et al.*, 1986, 1987]. The profiles were selected from the 7-year period of December 1975 to November 1982 and collected into monthly sets for marine and continental conditions (24 sets). In this study, only the marine data sets have been used, consisting of quality-controlled profiles for each month of the year, originating from ocean weather stations (OWS), islands, and coastal weather stations.

The initial selection was restricted to profiles which extended to pressure levels of 15 mbar or less and included moisture information (dew point temperature) to 600 mbar or less. One of the initial selection criteria was that the lowest level pressure measurement (P_0) be $\geq$ 1000 mbar. This was to ensure that the interpretation of computed correlations throughout the atmospheric column should not be confused by changes resulting from a reduced number of samples at $P_0 = 1000$ mbar. For the North Atlantic area as a whole this restriction does not introduce a significant sampling bias (see, for example, the charts of *Isemer and Hasse* [1985]), but this may not be the case in the GIN Sea area, particularly during winter. For example, at OWS "M" (66°N, 2°E) there is about an 8% probability of $P_0 <$ 1000 mbar during May, but in December the probability has increased to about 48% [*U.S. Naval Weather Service Command*, 1974*a*]. For some applications this

bias could be disturbing, while for others, including this study, the bias toward anticyclonic conditions with an increased likelihood of reduced cloud cover may reflect more appropriate sampling for infrared remote sensing.

The original monthly sets of marine atmospheric profiles consist of 400 ascents covering the area from about 30°N to 80°N, within a range of about 3000 km of the United Kingdom. For the purpose of simulating AVHRR/2 measurements in the GIN Sea area, radiosondes from stations north of 58°N and between 40°W and 20°E were selected. The number of radiosondes in each of the resulting monthly sets is given in Table 1, together with the mean values of some of the relevant atmospheric parameters, which are also shown graphically in Figure 3. It can be seen that February is the month with the driest atmosphere and lowest surface air temperature and July is the moistest and highest, which is in line with the North Atlantic region as a whole [*Minnett et al.*, 1987]. Profiles from these 2 months were selected to investigate the benefits of seasonal SST retrieval algorithms for AVHRR/2 measurements. Figure 4 shows the mean temperature and humidity profiles, with the envelope of ±1 standard deviation, for these months. These have been calculated after interpolating each measured profile to uniform pressure levels at 15 mbar resolution.

6.2. *Air–Sea Temperature Differences*

As discussed above, the temperatures measured in space are generally lower than the temperature of the sea surface. The size of this temperature deficit is strongly dependent on the difference between the surface air temperature and the SST. Furthermore, the retrieval coefficients optimized to give zero mean error when applied to measurements taken in a specific range of atmospheric conditions are themselves dependent on the air–sea temperature differences encountered in those conditions. Thus for the simulations to be accurate, realistic air–sea temperature differences must be used. (Unfortunately, the radiosonde profiles used here do not include the associated SST measurement).

The air–sea temperature difference field in most of the GIN Sea area is poorly sampled, especially in the winter months. An exception to this is the OWS "M," at 66°N, 2°E, and monthly statistics of surface meteorological variables are presented in graphic and tabular form by the *U.S. Naval Weather Service Command* [1974*a*, *b*]. Inspection of the tables of air-sea temperature differences for February and July [*U.S. Naval Weather Service Command*, 1974*b*] reveals that there are two distinct regimes in winter and summer. In February the SST is largely independent of surface air temperature, with low air temperatures being accompanied by large air–sea temperature differences: when the air temperature decreases, in the mean by 6.66 K, the SST is reduced by only 0.74 K. In July, however, a decrease in air temperature of 4.44 K is accompanied by an SST drop, in the mean, of 2.30 K. Such behavior is to be expected given the larger thermal inertia of the deeper surface mixed layer in winter.

For the AVHRR/2 simulations, it is appropriate therefore to associate each atmospheric profile with a set of SST values independent of the air temperature for February but to have sets of air–sea temperature differences which are dependent on the air temperature for July.

While it is reasonable to expect the distinct winter and summer regimes identified in the OWS "M" data to hold for the GIN Sea area as a whole, the SST values themselves at OWS "M" during February are patently inappropriate for other parts of the area: the mean SST being 6.5°C, with a standard deviation of only 0.7 K. This means, assuming a Gaussian distribution, that fewer than 1% of observations would be lower than 4.4°C, which is obviously not applicable in the northwest of the area toward the ice edge. Consequently, in what follows, SST values of −1.0°C, 1.0°C, 3.0°C, 5.0°C and 7.0°C are used with each atmospheric profile of the February simulations. These values encompass nearly all the range of February observations given in the US Naval weather atlas of the area [*U.S. Naval Weather Service Command*, 1974*a*], which shows the whole of the ice-free sea surface having mean temperatures in the range of -2°C to 8°C.

For the July simulations the air–sea temperature differences shown in Table 2 are used with each atmospheric profile. The values are derived from the OWS "M" data [*U.S. Naval Weather Service Command*, 1974*b*] and, since they are related to the surface

TABLE 1. Monthly Characteristics of the GIN Sea Marine Atmosphere

Month	Number of Profiles	Precipitable Water, kg m^{-2}	Surface Specific Humidity, g kg^{-1}	Surface Air Temperature, °C
Jan.	146	7.13 ± 3.82	3.16 ± 1.24	−0.02 ± 4.59
Feb.	183	6.26 ± 3.08	2.84 ± 1.10	−0.72 ± 4.75
March	148	6.46 ± 3.36	3.02 ± 1.23	−0.15 ± 6.52
April	175	7.31 ± 3.50	3.41 ± 1.40	1.22 ± 6.13
May	186	10.54 ± 5.13	4.42 ± 1.61	4.74 ± 5.78
June	148	15.31 ± 6.19	5.96 ± 1.86	8.74 ± 5.11
July	183	17.06 ± 5.14	6.57 ± 1.60	9.88 ± 4.26
Aug.	190	16.44 ± 5.75	6.43 ± 1.78	9.42 ± 4.48
Sept.	167	13.69 ± 6.12	5.41 ± 1.92	7.12 ± 4.87
Oct.	191	9.90 ± 4.88	4.24 ± 1.61	4.52 ± 4.88
Nov.	127	7.84 ± 4.15	3.48 ± 1.53	1.60 ± 5.17
Dec.	136	7.00 ± 3.55	3.18 ± 1.42	0.32 ± 4.74

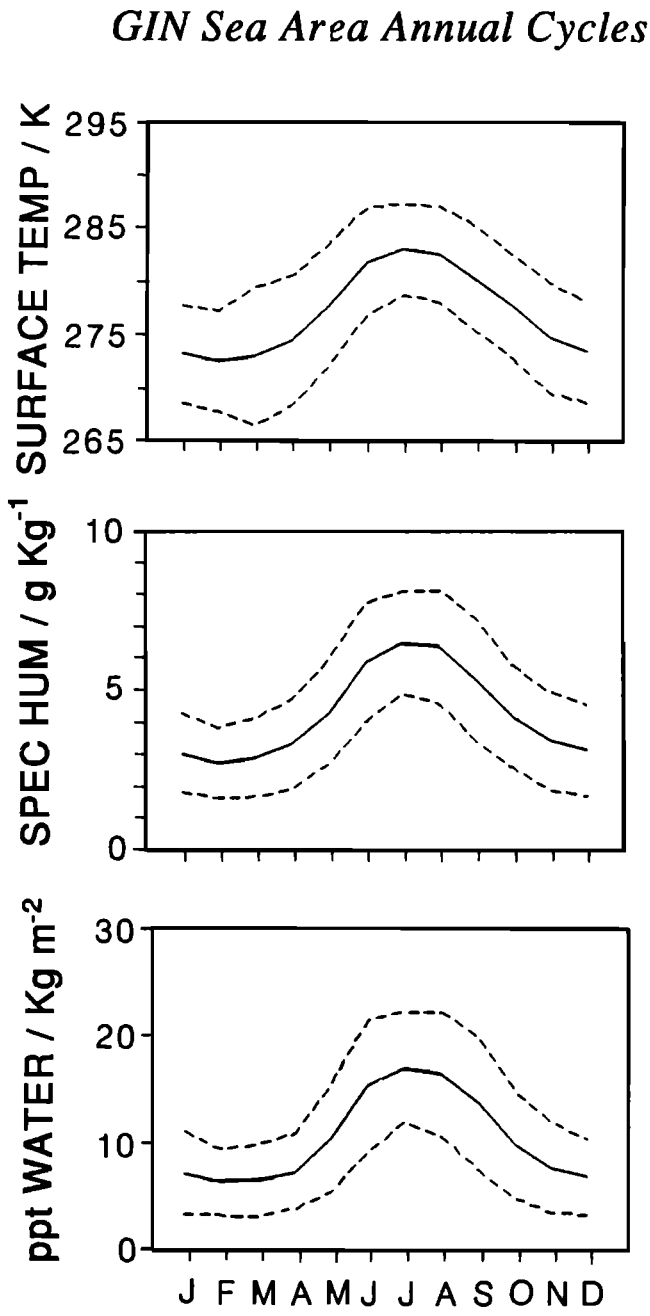

Fig. 3. Annual cycles of some atmospheric properties in the GIN Sea area. These are shown as monthly means ±1 standard deviations derived from radiosonde measurements. The variables are surface air temperature, surface specific humidity, and atmospheric water vapor column content (precipitable water). The numerical values are given in Table 1.

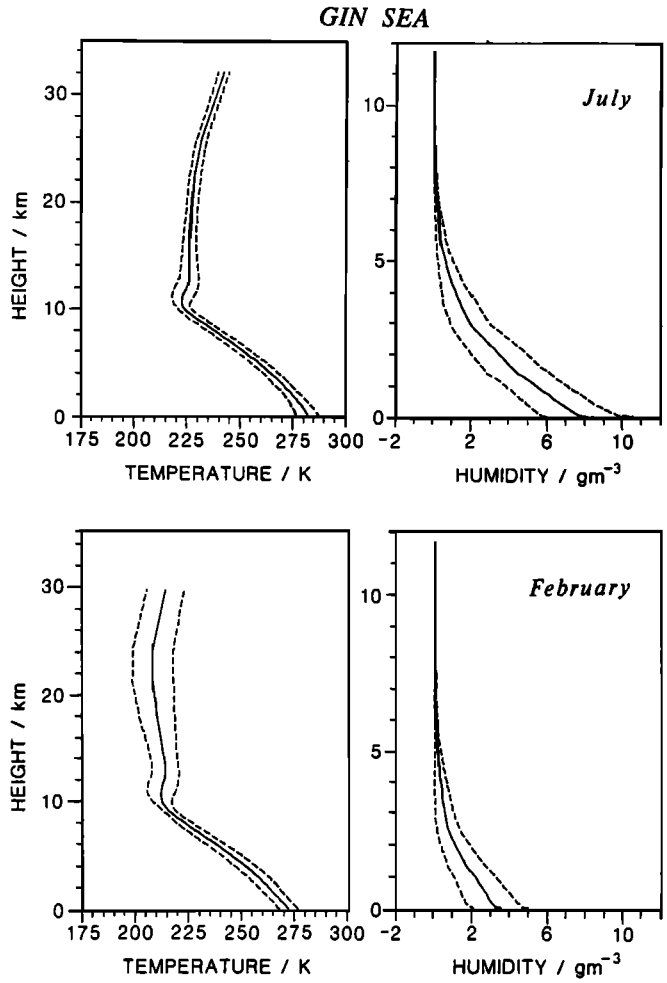

Fig. 4. Atmospheric profiles of temperature and absolute humidity for the summer (July) and winter (February) conditions in the GIN Sea area. The profiles are shown as mean values ±1 standard deviation for 15-mbar pressure increments of radiosonde profiles. The 1 standard deviation envelopes for the two seasons are exclusive.

air temperature of each profile, are taken to be applicable to the GIN Sea area as a whole.

6.3. *Tropospheric Aerosols*

Since the radiosonde profiles contain no information about the aerosol distribution in the atmosphere, a parameterization of aerosol effects in terms of the meteorological range is used (equation (8)). Estimates of visibility form part of the routine synoptic meteorological observations and their statistics have been compiled [*U.K. Meteorological Office*, 1964; *U.S. Naval Weather Service Command*, 1974*a*, *b*]. For the GIN Sea area, the available statistics are dominated by the observations from OWS "M" (66°N, 2°E), which show that when there is no precipitation (a necessary condition for infrared remote sensing), nearly half (~ 44%) of the observations have visible range > 30 n. mi., i.e. > 55 km [*U.K. Meteorological Office*, 1964]. This is also the case for the smaller number of reports from Jan Mayen Island [*U.K. Meteorological Office*, 1964]. The monthly mean visibilities at OWS "M" show some seasonal dependence with values of 10–12 n. mi. (18–22 km) in winter compared to 20 n. mi. (37 km) in early summer. These mean values are for all observations, however, and probably merely reflect the winter increase in the frequency of precipitation [*Gathman*, 1985].

However, the "visibility," which is subjectively determined, is not the same as the quantitative "meteorological range" required for the Koschmieder formula (equation (8)), the relationship between the two being

$$V = (1.3 \pm 0.3)V_{\text{obs}} \qquad (12)$$

where V_{obs} is the observed visibility [*Kneizys et al.*,1980].

TABLE 2. Air–Sea Temperature Differences Used in the July Simulations

Surface Air Temperature, °C	Air–Sea Temperature Difference, K				
	Δ_1	Δ_2	Δ_3	Δ_4	Δ_5
≤ 9.0	−3.0	−2.5	−2.0	−1.5	−1.0
> 9.0 to ≤ 11.5	−1.5	−1.0	−0.5	0.0	0.5
> 11.5	−1.0	−0.5	0.0	0.5	1.0

Positive air–sea temperature differences indicate air temperature higher than sea temperature.

For the simulations reported here, a meteorological range of 50 km has been used, which corresponds to an observed visibility of 30–50 km (17–26 n. mi.). In this respect the simulations will be of less favorable conditions than the mean.

7. The Advanced Very High Resolution Radiometer

The AVHRR/2 (advanced very high resolution radiometer) is a five-channel imaging device which forms part of the payload of the TIROS-N series of polar-orbiting weather satellites. There are two such satellites in operation at any time (currently NOAA 10 and NOAA 11) in Sun-synchronous orbits; one overhead at about 0230 UTC and 1430 UTC, and the other at about 0730 UTC and 1930 UTC. The satellites are about 840 km above the sea surface and have orbital periods of ~ 100 min. The channel characteristics are given in Table 3. However, it should be noted that the AVHRRs on TIROS-N, NOAA 6, NOAA 8 and NOAA 10 are without channel 5.

The AVHRR/2 data stream includes measurements in the infrared channels of an on-board black-body calibration target and of space (zero radiance measurement). The temperature of the black-body, which is close to terrestrial temperatures, is monitored by four platinum resistance thermometers. The noise levels in the two longwave channels is low, being given as 0.12 K for a 300 K target, but in reality they appear to be much lower. The data from each channel are digitized to 10-bit resolution (0–1023). The spatial resolution at nadir is 1.1 km, and the swath width is about 3150 km.

Information about the instrumental properties is published by NOAA as each new satellite becomes operational. The spectral response functions of the channels vary from instrument to instrument, which has a consequence on the SST retrieval expressions. Detailed descriptions of the AVHRR/2 instrument and data stream are given by *Schwalb* [1978] and *Lauritson et al.* [1979].

8. Results of GIN Sea Simulations

The results of the simulations of the AVHRR/2 split-window measurements for the Greenland–Iceland–Norwegian Sea conditions are presented in this section. Sea surface temperature retrieval coefficients are derived, and their error characteristics are discussed.

The values of the simulated temperatures for February (winter conditions) and July (summer conditions) are given in Table 4 as mean values and standard deviations for four different zenith angles (measured at the sea surface). The temperature deficits are also given in Table 4. The simulated values agree with physical expectations, in that (1) $T_5 < T_4$, (2) the temperature deficits become more negative with increasing zenith angles, (3) temperature deficits are more negative for summer conditions, when the atmospheric water vapor burden is greater, and (4) the variability of the temperature deficits is greater for channel 5 than for channel 4, reflecting the increased contribution of the atmosphere to the channel 5 signal.

That the variances of the measured temperatures are smaller than for the sea surface temperature confirms that the presence of the atmosphere attenuates the magnitude of surface temperature gradients when measured from space.

8.1. *Regionally Optimized Sea Surface Temperature Retrievals*

The simulated temperature measurements for the winter and summer conditions were regressed against the corresponding sea surface temperatures to derive the retrieval coefficients optimized for the GIN Sea area. These are given in Table 5 together with an estimate of the standard error of the retrievals, which is smallest for measurements at nadir ($\sec\theta = 1.0$). The coefficients are optimized for the conditions used in the simulations in that they produce a zero mean SST retrieval error and minimised standard error. The channel transfer functions of the NOAA 7 AVHRR/2 were used. A noise equivalent temperature difference (NEΔT) of 0.02 K was assumed for both channels in all cases, which is smaller than the single pixel value of 0.12 K. The small (NEΔT) requires the averaging of temperature measurements over at least 36 nearby pixels, thereby reducing the random instrumental contribution to the uncertainty in the retieved SST value; this is desirable for many applications, such as climate studies, where

TABLE 3. AVHRR Channel Characteristics

Channel	Wavelength, μm	Signal
1	~ 0.6 to ~ 0.7	reflected solar energy: clouds, coastlines, vegetation
2	~ 0.7 to ~ 1.1	reflected solar energy: clouds, coastlines, vegetation
3	~ 3.5 to ~ 4.0	reflected solar and thermal emission: clouds, SST
4	~ 10.3 to ~ 11.3	thermal emission: SST, clouds
5	~ 11.5 to ~ 12.5	thermal emission: SST, clouds

TABLE 4. Simulated NOAA 9 AVHRR Measurements Over GIN Sea

Zenith Angle θ, deg	$\sec\theta$	T_s, °C	T_4, °C	T_5, °C	$T_4 - T_s$, K	$T_5 - T_s$, K
			February			
0.0	1.00	3.000 ± 2.831	1.915 ± 2.693	1.550 ± 2.635	−1.085 ± 0.195	−1.450 ± 0.290
41.4	1.33	3.000 ± 2.831	1.554 ± 2.653	1.079 ± 2.581	−1.446 ± 0.253	−1.921 ± 0.368
53.1	1.67	3.000 ± 2.831	0.855 ± 2.604	0.209 ± 2.520	−2.145 ± 0.318	−2.791 ± 0.454
60.0	2.00	3.000 ± 2.831	−0.027 ± 2.554	−0.933 ± 2.460	−3.027 ± 0.393	−3.933 ± 0.563
			July			
0.0	1.00	10.516 ± 3.627	8.941 ± 3.445	8.333 ± 3.382	−1.575 ± 0.435	−2.183 ± 0.631
41.4	1.33	10.516 ± 3.627	8.489 ± 3.415	7.772 ± 3.359	−2.027 ± 0.548	−2.744 ± 0.773
53.1	1.67	10.516 ± 3.627	7.799 ± 3.418	6.985 ± 3.388	−2.717 ± 0.647	−3.531 ± 0.890
60.0	2.00	10.516 ± 3.627	7.033 ± 3.454	6.117 ± 3.468	−3.483 ± 0.734	−4.399 ± 0.991

The temperatures and temperature differences are given as mean ± standard deviation of 500 values, derived from simulations using 100 atmospheric profiles, each with five air–sea temperature differences.

TABLE 5. GIN Sea Area Sea Surface Temperature Retrieval Coefficients (Channels 4 and 5 of NOAA 7 AVHRR/2)

$\sec\theta$	a_0	a_4	a_5	σ, K
		February Conditions		
1.00	0.512	2.230	−1.281	0.08
1.33	0.619	2.479	−1.461	0.10
1.67	0.962	2.625	−1.603	0.12
2.00	1.457	2.618	−1.586	0.14
		July Conditions		
1.00	0.223	2.935	−1.933	0.12
1.33	0.264	3.110	−2.105	0.15
1.67	0.547	3.268	−2.257	0.19
2.00	0.890	3.393	−2.372	0.25

The coefficients are for temperatures expressed in degrees Celsius.

the high spatial resolution can be sacrificed, to some degree, for improved absolute accuracy.

In order to determine whether the effort of deriving regional coefficients is worthwhile, two sets of globally applicable retrieval coefficients were applied to the GIN Sea simulations. The first set of global coefficients is those used by NOAA for the operational generation of SST fields, known as the MCSST (multichannel sea surface temperature) maps, and is derived by regressing real satellite data with in-situ measurements from drifting buoys (McClain et al., 1985). Two different sets of MCSST coefficients are necessary for use with daytime and nighttime data. This reflects different satellite data processing schemes (i.e., in the identification of cloud contaminated pixels) for the two types of data, and since information from the shortwave channels is available for effective cloud detection during the day, it is presumed that the daytime coefficients are less likely to suffer from the effects of undetected cloud and more applicable to these simulations. Thus the daytime coefficients are used here (but in fact for NOAA 7 the differences in the coefficients for day and night use are small). The MCSST coefficients are given in Table 6 together with the errors, listed as means and standard deviations, that arise when they are applied to the GIN Sea simulations. Although the MCSST coefficients (Table 6) and those derived here (Table 5) are significantly

TABLE 6. GIN Sea Area Regional and Zenith Angle Dependences: Sea Surface Temperature Errors from Applying Global (MCSST) and Global, Zenith Angle Dependent (RAL) Coefficients to NOAA 7 AVHRR Simulations

MCSST*			RAL†		
$\sec\theta$	Mean	σ	$\sec\theta$	Mean	σ
		February Conditions			
1.00	−0.54	0.20	1.00	−0.45	0.17
1.50	−0.66	0.21	1.50	−0.63	0.26
2.00	−1.09	0.25	2.00	−0.60	0.43
		July Conditions			
1.00	0.09	0.24	1.00	−0.23	0.19
1.50	−0.38	0.23	1.50	−0.40	0.32
2.00	−1.19	0.26	2.00	−0.75	0.44

All temperature errors are in kelvin.

* The MCSST equation is $SST = -0.609 + 3.6125T_4 - 2.5779T_5$.

† The RAL equations are $SST = -0.528 + 3.7958T_4 - 2.8032T_5$ at $\sec\theta = 1.0$, $SST = -0.993 + 4.2990T_4 - 3.2978T_5$ at $\sec\theta = 1.5$, and $SST = -1.220 + 4.7108T_4 - 3.6895T_5$ at $\sec\theta = 2.0$.

different, the MCSST retrievals for July conditions at nadir are good, having only a small residual mean error. The mean errors increase with increasing zenith angle, as do the standard deviations. With the exception of July conditions at $\sec\theta = 2.0$, which show a large mean error, the standard deviations are generally more than twice as large as those of the optimized coefficients.

The second set of global coefficients has an explicit zenith angle dependence and was derived by *Llewellyn-Jones et al.* [1984] using the same radiative transfer model as is used here, with radiosonde profiles from the North Atlantic and the tropics. The differences between the earlier simulations of *Llewellyn-Jones et al.* [1984] and those presented here are in the environmental variables that describe different ranges of global and regional conditions. The *Llewellyn-Jones et al.* [1984] coefficients and the errors that result from their application to the GIN Sea simulations are also given in Table 6, where they are designated by "RAL." As expected, these coefficients reduce significantly the zenith angle dependence of the mean errors, but at the cost of increasing the zenith angle dependence of the scatter.

Both the MCSST and RAL global coefficients could be empirically adjusted to the GIN Sea conditions by incorporating the mean errors into the value of the a_0 coefficient. Even so, the residual scatter of the retrieved SSTs would still be about twice as large as that for the optimized coefficients. In such a case it is interesting to note that the adjusted MCSST coefficients, in which the zenith angle dependence is confined to the a_0 value, would perform better than the the adjusted RAL algorithm in which the zenith angle dependence is explicit in all coefficients.

8.2. *Seasonal Dependence*

The seasonal variations in the atmospheric temperature and humidity profiles are sufficiently great for the envelopes of ± 1 standard deviation about the mean profile to be exclusive (Figure 4). This is true also of the marine atmosphere over the NE Atlantic as a whole [*Minnett et al.*, 1987]. This seasonal variation suggests that there may be an advantage in having seasonally optimised coefficients. However, although such seasonal coefficients are significantly different from each other, the seasonal atmospheric variability is not sufficiently great for the improvement in accuracy to really require their use. This can be illustrated by applying the February coefficients to the July simulations and vice versa, the results of this test being shown in Table 7. These mean errors are small and would be yet smaller if a regional algorithm derived from an annual selection of radiosondes were to be used. This indicates that these regionally optimized coefficients are robust over the range of atmospheric conditions experienced in the course of the seasonal cycle described here.

TABLE 7. Seasonal Dependence of Temperature Errors Caused by Applying February Coefficients to July Simulations (NOAA 9)

$\sec\theta$	Mean	σ
1.00	−0.02	0.18
1.33	−0.05	0.22
1.67	−0.10	0.24
2.00	−0.17	0.33

All temperature errors are in kelvin.

8.3. *Zenith Angle Dependence*

The need to account for the zenith angle dependence of the retrieval coefficients in accurate SST measurement has been stressed by a number of authors, particularly *Llewellyn-Jones et al.* [1984]. Indeed, *Saunders* [1967] found that, for airborne measurements, increasing the zenith angle from 0° to 60° practically doubled the temperature deficit and thereby suggested a mechanism for correcting for the atmospheric effect.

The consequence of failing to account for the changing zenith angle across the swath is already apparent in the discussion of the global algorithms (Table 6), but in order to investigate the magnitude of the effect in the case of optimized coefficients, each set of coefficients for the four zenith angles used in the simulations was applied to every set of simulated measurements. The resulting errors are shown in Table 8, which illustrates that failure to account properly for the zenith angle dependence can lead to unacceptable errors.

In reality the effects of zenith angle change smoothly across the swath, which suggests that a functional dependence on zenith angle of the retrieval might be expected. However, there are two factors involved: the increasing atmospheric path length with increasing zenith angle, and the decrease in surface emissivity with increasing emission (or zenith) angle, which in turn changes the effective air–sea temperature difference. Thus for the general case where the atmosphere is cooler than the sea surface, the effective air–sea temperature difference becomes less negative away from the center of the swath. If the air were only slightly cooler than the skin SST, the decrease in the radiation temperature at high emission angles might even cause the temperature difference between the air and the emitted radiation to change sign across the AVHRR swath. Thus the effect of the lower layers of the atmosphere would be to decrease the apparent radiation temperature of the upwelling radiation at nadir but to increase it toward the edges of the swath. The relative contributions of the emissivity and atmosphere to the mean temperature deficit are shown for the February simulations in Table 9, from which it can be seen that in this case, the emissivity effects are dominant.

In order to demonstrate that for the GIN Sea area at least, the zenith angle dependence of the optimized retrieval coefficients is adequately described by a choice of four zenith angles, a set of simulations for $\sec\theta$=1.50 were made. The errors resulting from applying coefficients for this zenith angle derived by linear interpolation between $\sec\theta$=1.33 and $\sec\theta$=1.67 were calculated and are shown in Table 10. These errors are small enough to be neglected, and if a higher-order expression were to be used for the interpolation, these errors would be yet smaller.

8.4. *Instrumental Dependence*

The channel response functions vary from instrument to instrument, sometimes by design to improve the performance of the instrument, and at other times unin-

TABLE 8. Zenith Angle Effects: Mean Sea Surface Temperature Errors from Failure to Account for Zenith Angle Dependency (Channels 4 and 5 of NOAA 9, July Conditions)

Simulation ($\sec\theta$)	Coefficient ($\sec\theta$)			
	1.00	1.33	1.67	2.00
1.00	0.00	0.21	0.67	1.19
1.33	−0.27	0.00	0.17	1.00
1.67	−0.76	−0.48	0.00	0.53
2.00	−1.32	−1.03	−0.54	0.00

All temperatures are in kelvin.

TABLE 9. Zenith Angle Effects: Surface Emissivity and Atmosphere for February Conditions

$\sec\theta$	$T_s - T_i$,* K	ϵ	δT_ϵ,† K	δT_a,‡ K
		Channel 4		
1.0	1.085	0.990	0.57	0.52
2.0	3.027	0.960	2.29	0.74
		Channel 5		
1.0	1.450	0.986	0.86	0.59
2.0	3.933	0.947	3.32	0.61

* Here, $i = 4, 5$.

† Temperature drop due to deviation from unity of surface emissivity ϵ.

‡ Temperature drop due to atmospheric effects.

tentionally through slight variations in the properties of filters and detectors. For example, the NOAA 9 AVHRR/2 channel transfer functions are shifted slightly to higher wave numbers compared with those of the instrument on NOAA 7: by ~ 5 cm^{-1} for channel 5 and ~ 2 cm^{-1} for channel 4. The widths of the corresponding channels are similar for each instrument, but the positions of local maxima (i.e., peak transmissions) have changed for channel 5. The net effect is that the same radiance measured by the two instruments corresponds to different temperatures. The NOAA 9 channel 4 temperatures are about 0.2 K lower than those of NOAA 7, and this difference is practically independent of temperature, while channel 5 temperatures are about 0.2 K higher for a measurement at 310 K, but the difference decreases to zero at about 270 K.

It is generally accepted that different retrieval coefficients are required for each instrument and hence, for example, new sets of MCSST coefficients are issued for each satellite. The loss of accuracy resulting from failing to account for the different satellite characteristics can be quantified by applying coefficients derived using the NOAA 9 transfer functions to the NOAA 7 simulations. These errors are shown in Table 11. They are generally greater than those resulting from failure to account for the seasonal dependence (Table 7) but much smaller than those caused by failing to account for the zenith angle dependence (Table 8) or by using global algorithms (Table 6).

9. SUMMARY AND CONCLUSIONS

The measurements of the AVHRR/2 thermal infrared channels (4 and 5 at ~ 10 μm to ~ 13 μm wavelength) have been simulated by a line-by-line radiative transfer model using realistic atmospheric and oceanic parameters characteristic of the Greenland-Iceland-Norwegian Sea region.

The simulations have been used to derive sea surface temperature retrieval coefficients that are optimized for the winter (February) and summer (July) conditions of the GIN Sea area. The retrieval coefficients have an explicit zenith angle dependence to account for the changing surface emissivity and atmospheric path length across the swath.

A number of approaches for improving the error characteristics of satellite-derived SSTs in a regional study have been explored, and the benefits of each have been quantitatively assessed to determine their relative merits. These approaches are, in the order in which they improve the error characteristics:

TABLE 10. Zenith Angle Effects: Errors from Interpolating Coefficients at $\sec\theta = 1.50$

	a_0	a_4	a_5	ϵ, K*	σ, K
		February			
Simulated	0.796	2.637	−1.612	–	0.114
Interpolated	0.859	2.630	−1.605	0.059	–
		July			
Simulated	0.411	3.338	−2.324	–	0.171
Interpolated	0.479	3.335	−2.321	0.065	–

* Mean error in applying interpolated coefficients to simulated brightness temperatures.

TABLE 11. Spacecraft Dependence: Sea Surface Temperature Errors from Applying NOAA 9 Coefficients to NOAA 7 Simulations

sec θ	Mean	σ
	February Conditions	
1.00	0.076	0.085
1.33	0.109	0.103
1.67	0.137	0.121
2.00	0.142	0.144
	July Conditions	
1.00	0.170	0.122
1.33	0.223	0.158
1.67	0.265	0.201
2.00	0.290	0.255

All temperatures are in kelvin.

1. Zenith angle dependence: Failure to account for the dependence of the retrieval coefficients can lead to mean errors in excess of 1 K if, for example, coefficients derived for near-nadir measurements are applied to measurements toward the edge of the swath. Of the zenith angle effects, that of the changing surface emissivity can be more important than that caused by increased atmospheric path length. It is sufficient to derive the retrieval coefficients at only four distinct zenith angles ($\sec^{-1}$ 1.00, 1.33, 1.67, and 2.00 have been used here) and interpolate to all other zenith angles. Linear interpolation appears to be adequate. Admittedly, some sets of coefficients (such as those of the MCSST) are intended for application to data in a reduced range of zenith angles, close to nadir, but in geographical areas where cloud cover can severely restrict the number of occasions when the sea surface can be sampled (such as the GIN Sea area) the luxury of discarding cloud-free parts of the image because they lie toward the edges of the swath can be ill-afforded.

2. Regional dependence: The application of coefficients intended for global use in a regional study, such as of the GIN Sea area, can result in mean errors up to 1 K. The errors show a distinct zenith angle dependence.

3. Seasonal dependence: The failure to account for the seasonal changes in the atmospheric conditions results in quite small mean errors. For example, applying coefficients derived from simulated measurements through the cold, dry atmospheres of February to the simulated data from the (relatively) warm, moist atmospheres of July results in mean errors of only a few tenths of a degree.

4. Spacecraft dependence: It is generally acknowledged that individual sets of coefficients are required for each instrument, but for the GIN Sea conditions at least, the mean errors that arise when NOAA 9 coefficients are applied to NOAA 7 simulated data are small in the mean, being about twice those caused by the neglect of the seasonal effects.

While much effort has been invested in ensuring that the model and input data provide a realistic representation of the physical world, there is always the risk that some factor is missing or inadequately treated, especially when there are insufficient independent data (such as in-situ measurements) with which to conduct a definitive test. Such is the case with this study. The radiosondes used here have been subjected to careful quality control and are used only to describe the atmosphere in a statistical sense and not to describe the state of the atmosphere at the time and place of measurement of each profile. Thus individual random measurement errors do not invalidate the results. The surface pressure bias in the radiosondes of the winter months (see above) is also unlikely to have unduly influenced the results: the only consequence is to have diminished the effects of seasonal changes, but even then, by a factor of probably less than 2.

Because the atmospheric profiles and other variables are believed to give an accurate, statistical description of the environmental conditions, it is legitimate to draw the comparision between the results of regional algorithms, internal to the set of simulations described here, and those of global algorithms obtained independently of these simulations.

The somewhat surprising result that the effects of seasonal environmental changes are small compared with those attributed to regional variations indicates that the seasonal changes in this area are much smaller than the departure of the regional conditions from those appropriate to the "global" coefficients (RAL and MCSST), which are obviously influenced by the warmer, moister atmospheres of the tropics and subtropics. A corresponding study aimed at a different region, such as the tropics, might show the seasonal variations to be more important than they are at these high latitudes.

This study has been confined to a well-defined geographic region and an extension of this approach to optimizing satellite SST retrievals to larger areas is a suitable topic for further research, especially to determine the correct criterion for matching the retrieval coefficients to the changing environmental conditions over the global ocean.

The accuracy required of satellite measurements of sea surface temperature depends, of course, on the intended applications. For some purposes it may be acceptable to neglect some of the dependences discussed above. But in any event, the merit of using optimised, zenith-angle dependent, split-window coefficients in regional studies has been clearly demonstrated.

Acknowledgments. Thanks are due to A. M. Zavody of the Rutherford Appleton Laboratory (RAL) of the U.K. Science and Engineering Research Council, for advice on radiative transfer modelling, for supplying the precomputed spectral parameters, and for useful comments on an earlier draft of this paper; and to D. T. Llewellyn-Jones, Head of Atmospheric Sciences at RAL, for permission to use the model.

REFERENCES

Barton, I. J., A. M. Zavody, D. M. O'Brien, D. R. Cutten, R. W. Saunders, and D. T. Llewellyn-Jones, Theoretical algorithms for satellite-derived sea surface temperature, *J. Geophys. Res., 94*, 3365–3375, 1989.

Bernstein, R. L., Sea surface temperature estimation using the NOAA-6 satellite advanced very high resolution radiometer, *J. Geophys. Res., 87*, 9455–9465, 1982.

Bohlander, R. A., Spectroscopy of water vapour, Ph.D. thesis, Univ. of London, London, 1979.

Coakley, J. A., and F. P. Bretherton, Cloud cover from high resolution scanner data: Detecting and allowing for par-

tially filled fields of view, *J. Geophys. Res., 87*, 4917–4932, 1982.

Crosby, D. S., and K. S. Glasser, Radiance estimates from truncated observations, *J. Appl. Meteorol., 17*, 1712–1715, 1978.

Gathman, S. G., Climatology, in The Nordic Seas, edited by B. G. Hurdle, pp. 1–18, Springer-Verlag, New York, 1985.

Gross, E. P., Shape of collision-broadened spectral lines, *Phys. Rev., 97*, 395–403, 1955.

Hänel, G., The properties of atmospheric aerosol particles as functions of the relative humidity at thermodynamic equilibrium with the surrounding moist air, *Adv. Geophys., 19*, 73–188, 1976.

Hanson, K. J., J. T. Peterson, J. Namias, R. Born, and C. S. Wong, On the influence of Pacific Ocean temperatures on atmospheric carbon dioxide concentration at Ocean Weather Station 'P', *J. Phys. Oceanogr., 11*, 905–912, 1981.

Isemer, H. J., and L. Hasse, *The Bunker Climate Atlas of the North Atlantic Ocean*, vol. 1, *Observations*, 218 pp., Springer-Verlag, New York, 1985.

Kneizys, F. X., E. P. Shettle, W. O. Gallery, J. H. Chetwynd, L. W. Abreu, J. E. A. Selby, R. W. Fenn, and R. A. McClatchey, Atmospheric transmittance/radiance: Computer code LOWTRAN 5, *Rep. AFGL-TR-80-0067*, 233 pp., Air Force Geophys. Lab., Hanscom Air Force Base, Mass., 1980.

Kondratyev, K. Ya., *Radiation in the Atmosphere*, pp. 161–171, Academic, San Diego, Calif., 1969.

Lauritson, L., G. J. Nelson, and F. W. Porto, Data extraction and calibration of TIROS-N/NOAA radiometers, *NOAA Tech. Memo. NESS 107*, Nat. Oceanic and Atmos. Admin., Washington, D.C., 1979.

Llewellyn-Jones, D. T., P. J. Minnett, R. W. Saunders, and A. M. Zavody, Satellite multichannel infrared measurements of sea-surface temperature of the N.E. Atlantic Ocean using AVHRR/2, *Q. J. Roy. Meteorol. Soc., 110*, 613–631, 1984.

McClain, E.P., W. G. Pichel, and C. C. Walton, Comparative performance of AVHRR-based multichannel sea-surface temperatures. *J. Geophys. Res., 90*, 11,587–11,601, 1985.

McMillin, L., Estimation of sea surface temperatures from two infrared window measurements with different absorption, *J. Geophys. Res., 80*, 5113–5117, 1975.

McMillin, L. and D. S. Crosby, Theory and validation of the multiple window sea surface temperature technique, *J. Geophys. Res., 89*, 3655–3661, 1984.

McMillin, L. and D. S. Crosby, Some physical interpretations of statistically derived coefficients for split-window corrections to satellite derived sea surface temperatures, *Q. J. Roy.Meteorol. Soc., 111*, 867–871, 1985.

Minnett, P. J., A numerical study of the effects of anomalous North Atlantic atmospheric conditions on the infrared measurement of sea surface temperature from space, *J. Geophys. Res., 91*, 8509–8521, 1986.

Minnett, P. J., The numerical simulation of infrared satellite measurements over the Greenland-Iceland-Norwegian Sea, *Rep. SR-137*, 61 pp., SACLANT Undersea Research Centre, La Spezia, Italy, 1988.

Minnett, P. J., A. M. Zavody, and D. T. Llewellyn-Jones, Satellite measurement of sea-surface temperature for climate research, in Large-scale oceanographic experiments and satellites, edited by C. Gautier and M. Fieux, pp. 57–85, D. Reidel, Hingham, Mass., 1984.

Minnett, P. J., J. R. Eyre, and R. W. Pescod, The marine atmosphere over the northeastern Atlantic Ocean: a monthly description of some variables relevant to satellite remote sensing of the ocean and atmosphere. *Rep. RAL-86-044*, 75 pp., Rutherford Appleton Lab., Chilton, Oxfordshire, England, 1986.

Minnett, P. J., J. R. Eyre, and R. W. Pescod, The variability of the North Atlantic marine atmosphere and its relevance to remote sensing, *Int. J. Remote Sens., 8*, 871–880, 1987.

Phulpin, T., M. Derrien, and A. Brard, A two-dimensional histogram procedure to analyze cloud cover from NOAA satellite high-resolution imagery, *J. Clim. Appl. Meteorol., 22*, 1332–1345, 1983.

Prabhakara, C., G. Dalu, and V. G. Kunde, Estimation of sea–surface temperature from remote sensing in 11 to 13μm window region, *J. Geophys. Res., 80*, 5039–5044, 1974.

Robinson, I. S., N. C. Wells, and H. Charnock, The sea surface thermal boundary layers and its relevance to the measurement of sea surface temperature by airborne and spaceborne radiometers, *Int. J. Remote Sens., 5*, 19–46, 1984.

Rothman, L. S., AFGL atmospheric absorption line parameters compilation: 1980 version, *Appl. Opt., 20*, 791–795, 1981.

Saunders, P. M., Aerial measurements of sea-surface temperatures in the infrared, *J. Geophys. Res., 72*, 4109–4117, 1967.

Saunders, R. W., An automated scheme for the removal of cloud contamination from AVHRR radiances over western Europe, *Int. J. Remote Sens., 7*, 867–886, 1986.

Saunders, R. W. and K. T. Kriebel, An improved method for detecting clear sky and cloudy radiances from AVHRR data, *Int. J. Remote Sens., 9*, 123–150, 1988. (Correction, *Int. J. Remote Sens., 9*, 1393–1394, 1988.)

Schluessel, P., H.-Y. Shin, W. J. Emery, and H. Grassl, Comparison of satellite-derived sea-surface temperature with in-situ skin measurements, *J. Geophys. Res., 92*, 2859–2874, 1987.

Schwalb, A., The TIROS-N/NOAA A-G satellite series, *NOAA Memo NESS 95*. 80 pp., Nat. Oceanic and Atmos. Admin.,Washington, D.C., 1978.

Tiwari, S. N., Models for infrared atmospheric radiation, *Adv. Geophys., 20*, 1–85, 1978.

United Kingdom Meteorological Office, Weather in Home Fleet Waters, vol. 1, The Northern Seas, part 1, *Publ. M O 732(a)*, 230 pp., HMSO, London, 1964.

United States Naval Weather Service Command, Marine climatic atlas of the world, vol. 1, North Atlantic Ocean, *Rep. NAVAIR 50-1C-528*, 371 pp., U. S. Govt. Print. Off., Washington D.C., 1974*a*.

United States Naval Weather Service Command, Summary of synoptic meteorological observations, Western European coastal marine areas, vol. 7, 499 pp., Nat. Clim. Center, Asheville, N.C., 1974*b*.

P. J. Minnett, Oceanographic and Atmospheric Sciences Division, Department of Applied Science, Brookhaven National Laboratory, Upton, NY 11973.

(Received November 2, 1988;
accepted April 24, 1990.)